Cronfa - Swansea University Open Access Repository

_____

This is an author produced version of a paper published in :
Proceedings of Computer Graphics and Visual Computing (CGVC) 2014

Cronfa URL for this paper:

_____

Conference contribution :

_____

Comparative Visualization and Analysis of Time-Dependent, 2D Foam Simulation Data

Dan R. Lipşa[1,3], Robert S. Laramee[1], Simon Cox[2], and I. Tudur Davies[2]

[1]Swansea University, U.K., E-mail: r.s.laramee@swansea.ac.uk
[2]Aberystwyth University, U.K., E-mails: {foams, itd}@aber.ac.uk
[3]Kitware, Inc., U.S.A, E-mail: dan.lipsa@kitware.com

Abstract
Liquid foams have important practical applications. To analyze the dependence of foam behavior on material properties, and to improve foam models, foam scientists work with dozens of related simulations obtained by varying these material properties as well as parameters such as foam attributes, properties of objects interacting with foam or shape of foam containers. We present visualization solutions, developed in close collaboration with foam scientists, designed to compare and analyze related simulations. We evaluate our solutions by deploying them at the scientists' site. We demonstrate their effectiveness through results obtained by domain experts using our tool which include new findings and new approaches to analyze foam simulations. We propose a novel interaction and processing technique that enables the comparison of related events in different simulations and facilitates the examination of the temporal context for the events.

Categories and Subject Descriptors (according to ACM CCS): I.3.4 [COMPUTER GRAPHICS]: Graphics Utilities—Application packages

1. Introduction and Motivation

Liquid foams have important practical applications in areas such as oil recovery and mineral separation, food and beverage production, cleaning and fire extinguishing. Foam research can help to improve the quality of products and efficiency of processes in these areas by predicting and controlling foam behavior. In mineral separation ground ore is washed with foam. The efficiency of the separation of mineral from rock depends on how particles with different properties interact with foam. Scientists idealize this process by considering falling discs or ellipses in an otherwise stationary foam. For enhanced oil extraction, foam is pushed through porous rock to displace oil. Domain experts want to understand how the tortuous geometry of the rock pores affects the flow of foam. Domain experts idealize this process by studying foam flow through a constriction. When forced to flow through a constricted channel, many complex fluids, such as polymer melts, show regions in which material circulates in the upstream corners (salient corner vortices). As a consequence, material issuing from the channel can show markedly different ages, and therefore possibly different properties, and the flow-rate for a given pressure drop

will change. In the case of foams, such recirculation may lead to particles dropping out of the foam before they can be captured or, in the case of food foams, material becoming unusable because of its age. Scientists are interested in determining if and when such recirculation occurs for various channel geometries. During the processing of many materials, including foams, extrusion is often used to fill moulds and trigger foaming. The constriction simulations (Sec. 3) idealize this process, and start to tackle the question of how to design an optimal container shape to deliver the foam in such a way that its properties, such as bubble size and deformation, are controlled.

Transient liquid foam behavior is not well understood. The main goal of foam research is to determine foam behavior from measurable properties such as bubble size and its distribution, liquid fraction, and surface tension. One way to study this dependence is to simulate foam at the bubble level. This type of simulation makes it possible to model foam properties and see their influence on general foam behavior, to better inform continuum models of foam dynamics, and to make direct comparison with experiments. However, it also poses challenges for visualizing and inferring the gen-

eral foam behavior, as there is a high level of detail, data is temporal, and there are large fluctuations in values of bubble attributes.

In previous work, Lipşa et al. [LLCD11] presented FoamVis, an exploration, visualization and analysis application for foam simulation data. While this tool proved useful, important foam research questions are not addressed, as described next. Foam scientists work with dozens of simulations with a wide range of simulation parameters. Examples include foam container properties (such as channel geometry), foam attributes (such as bubble size and distribution, liquid fraction and surface tension) or the properties of objects interacting with foam (such as particle shape, size or position). The goal of varying these parameters is to model the foam response and to validate simulation against experiments. The large number of existing simulations and the variety of simulation parameters makes it difficult to manage simulation data and to understand the influence that simulation parameters have on foam behavior.

Previous tools do not support comparison of related simulations and only partially support domain scientists' analysis requirements. This work concentrates on these important challenges. Specifically we make the following contributions:

- We provide foam scientists with visualizations designed to enable comparison of related simulations and enhance their analysis capabilities. Comparative visualization features include: the two halves view, linked time with event synchronization, the reflection feature, force difference and torque visualizations. In this process we expand FoamVis' analysis and visualization capabilities and address limitations in the previous version [LLCD11]. Additional features include: deformation tensor computation and visualization using ellipses, time-average computation for vector and tensor simulation attributes, velocity vector visualizations using glyphs and streamlines, average around moving objects and, topological changes kernel density estimate visualization.
- We evaluate the proposed solutions by deploying them at the scientists' site. We demonstrate their effectiveness with results obtained by domain experts. First, areas of recirculation in the corners of a constricted channel are shown to exist, a result never presented before. Second, the sedimenting discs simulation is analyzed in a new way by comparing it with a sedimenting ellipse simulation. These analyses generate new research hypotheses for foam scientists.
- We present a novel interaction and processing technique, *linked time with event synchronization*, that enables the comparison of events in related simulations and facilitates the examination of their temporal context. We evaluate our technique using an example from foam simulation data.

The rest of this paper is organized as follows: Section 2

presents related work and Section 3 briefly describes the simulation datasets used in this paper. We present techniques that enable effective comparison between related simulations in Section 4 and visualizations designed to expand foam scientists' analysis capabilities in Section 5. We describe results obtained using our tool in Section 6, and end with conclusions and future work in Section 7.

2. Related Work

While some work that focuses on visualization of static foam or foam-like structures has been published, very little work in visualization of time-dependent, physically-accurate foam simulation data appears in the literature [LLC*12].

Comparative visualization refers to the process of understanding the similarities or differences between data from different sources. Differences between simulations and experiments, or between simulations or experiments with different parameters may be of interest. Such analysis can happen at different levels: image, data, derived quantities, and methodology levels. At the image level, the two sources can be compared by using two visualization images shown side by side [AHP*10], superimposed [PP95], as two symmetrical halves or by computing the difference between the two images. If images from several sources need to be compared, a space filling tilling can be used [MHG10]. At data level, data fields from the two sources are combined to produce a new visualization. Derived quantities or features can be extracted and compared, for instance streamlines in a vector field, vortex and shock wave positions [PW95] or detected edges in slices of an industrial scan [MHG10]. Differences in experiment, simulation or visualization parameters may be quantified and compared.

The goals of the reviewed works in comparative visualization are to find the optimal solution from a number of datasets or to understand how the datasets are different. For our work, the goal is to improve understanding of foam behavior, and as a result, produce better foam models. To reach this goal, we use a number of comparative visualization techniques designed to reduce the cognitive load required to integrate two side-by-side views, and we propose a new interaction and processing technique that allows scientists to compare events in related simulations while facilitating the examination of the temporal context for the events.

3. Foam Simulation Cases

A dry 2D foam at equilibrium consists of gas bubbles surrounded by films that are circular arcs which meet 3-way at angles of $120°$. Domain scientists simulate quasi-static flows of foams at the bubble-scale as described next. The initial structure for each simulation is created from a Voronoi tessellation of the unit square, with random seeds and periodic boundary condition, followed by a minimization of total film length. For each step, a line of films spanning the channel is
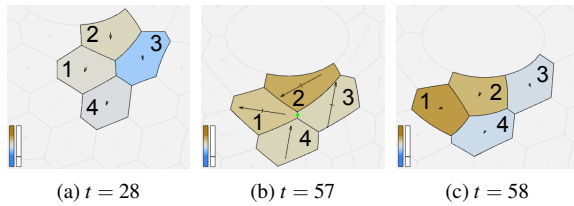
(a) $t = 28$ (b) $t = 57$ (c) $t = 58$

Figure 1: Topological change. We show three different time steps (in the *sedimenting-ellipse* simulation), bubbles color-mapped by pressure and velocity shown using arrows. In Fig. 1a bubble edges meet 3-way, with bubbles 1 and 3 adjacent (we choose t=28 as opposed to t=56 to emphasize the evolution of the four bubbles). As the falling ellipse compresses the bubbles, the film shared by bubbles 1 and 3 decreases in length (Fig. 1b), until the four bubbles move to an unstable configuration in which edges meet 4-way. Note the high velocity that bubbles have after the topological change. Fig. 1c shows the four bubbles after the topological change where bubbles 2 and 4 are adjacent, and edges meet 3-way.
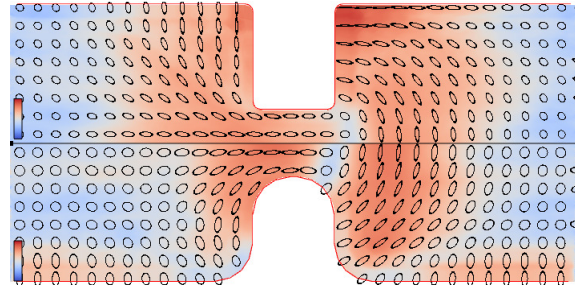

Figure 2: We show the square (top) and rounded (bottom) constriction simulations. Foam flows from left to right. Deformation size and direction is displayed with ellipses, deformation size is also color-mapped (with red for high and blue for low deformation). An average over the entire duration of the simulations is displayed. Rounding the corners of the constriction results in reduced elastic deformation of the foam (top versus bottom). In both simulations, there is an area where bubbles are not deformed (ellipses become circular) just downstream from the constriction.

moved downstream by a small distance (constriction); or an object in foam is moved a small distance in the direction of the resultant force on it. In both cases, this motion is followed by a reduction of the film length to a local minimum subject to prescribed bubble areas. During this minimization, topological changes (T1s) are triggered (see Fig. 1). A foam stored in a simulation file is always at equilibrium and it hops between equilibria in a quasi-static fashion. Thus we use time in an informal way to refer to the number of equilibration steps.

When a foam is subjected to stress, bubbles deform (elastic deformation) and rearrange (plastic deformation). Domain experts are interested in the distribution of the plasticity, which is indicated by the location of topological changes. A topological change (T1) is a neighbor swap between four neighboring bubbles as shown in Fig. 1: In a stable configuration, bubble edges meet 3-way at $120°$ angles. As the foam is sheared, bubbles move into an unstable configuration, in which edges meet 4-way, then quickly form a stable configuration again. The simulation code saves the time step and the *x*, *y* coordinates of the unstable intersection point for each topological change.

We use two simulation groups containing related simulations: constriction and sedimenting objects. The simulations in both groups are periodic in the direction of motion. The constriction simulation group contains two simulations, one with a *square-constriction* and one with a *rounded-constriction* (Fig. 2). They simulate a 2D polydisperse (bubbles with different volumes) foam flowing through a constricted channel, with 725 bubbles and 1000 time steps. The channel has unit length and the length of the constricted region is 0.148. Its width is 0.5 and the width of the constricted

region is 0.24. The simulations differ from each other in the geometry of the constriction. The radius of the circles creating the rounded corners of the constriction is 0.014 for the square-constriction and 0.069 for the rounded-constriction.

The sedimenting-objects simulations group contains the *sedimenting-ellipse* and the *sedimenting-discs* simulations (Fig. 3). We wish to understand the interaction between two sedimenting discs by comparing it with the (simpler) behavior of a sedimenting ellipse. *Sedimenting-discs* simulates two discs falling through a monodisperse (bubbles having equal volume) foam under gravity. It contains 330 time steps and simulates 2200 bubbles. The two discs are initially side-by-side and in close proximity. As they fall, they interact with the foam and with each other and rotate towards a stable orientation in which the line that connects their centers is parallel to gravity. There are two forces acting on each disc in addition to its weight. A pressure force results from each adjacent bubble pushing against it, while a network force arises because each contacting soap film pulls normal to the circumference with the force of surface tension. Due to the flow, the distribution of films and bubbles pressures around each disc is not uniform (for example, there is a high density of films above each disc, leading to a large, upward, network force there), resulting in a non-zero resultant force. *Sedimenting-ellipse* simulates an ellipse falling through a monodisperse foam under gravity. This group contains 540 time steps and simulates 600 bubbles. The major axis of the ellipse is initially horizontal. As the ellipse falls, it rotates toward a stable orientation in which its major axis is parallel to gravity. As for the sedimenting discs, a network and pressure force act on the ellipse and, due to its shape, they give rise to a non-zero torque that rotates it. We seek to validate
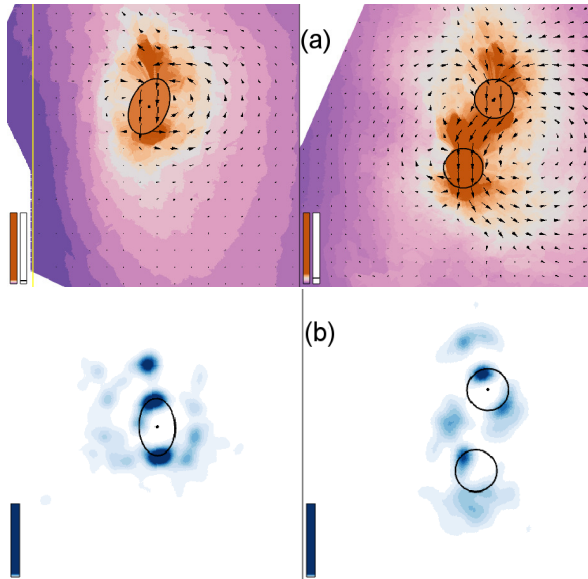
Figure 3: Sedimenting-ellipse versus sedimenting discs. (a) Visualization of velocity average, time window of 30 time steps, *around* the ellipse and the two discs, that uses the linked time with event synchronization feature (the ellipse and the two discs reach orientations 0° 30°, 60° and 90° in the same time). Velocity is displayed using glyphs and velocity magnitude is also color-mapped (with orange for high and purple for low velocity magnitude). The foam between the discs moves at high velocity with the discs which creates a similar velocity field as for the falling ellipse. (b) Few topological changes (T1s) occur between the discs, so foam in that region behaves mainly as an elastic solid. Topological changes *around* the ellipse and the two discs (Sec. 5.3), over the entire duration of the simulations, visualized using KDE. Both (a) and (b) use the *show rotation* option to render the rotation context for the ellipse and the discs.

the idea that the anisotropic two disc system responds to the foam-induced forces in the same way as an elliptical object.

For these simulations, we address a number of research questions. Do the two discs act as a large ellipse so is it possible to think of a torque acting on the system? If the answer to this question is positive, this will explain the complex behavior of two discs sedimenting in foam, where one disc rotates around the other. For the constriction simulations how does the foam respond to differences in container shape, and can it lead to non-trivial flow, such as recirculation and the recycling of material? In general - under what circumstances does a foam respond plastically or elastically? How does changing the container, or the object shape, affect that balance?

4. Comparative Visualization

Foam scientists often generate related simulations to study how varying just one of the many possible parameters affects the result. Examples of simulation parameters include foam container properties, foam attributes or the properties of objects interacting with foam. We modified FoamVis to enable loading and visualizing several simulations datasets at the same time. This feature is essential for comparing related simulations. We present the *two halves* view and the *linked time with event synchronization* features which address two orthogonal challenges in comparing simulations: space and time. We use the reflection feature and the force difference to facilitate the comparison of two datasets.

4.1. The two halves view

The *two halves* view facilitates visual comparison of two related foam simulations (Figures 2, 4, 6). It visualizes related simulations that are assumed to be symmetric with respect to one of the main axes. While the same information can be gathered by examining the two simulations in different views, the *two halves* view may facilitate analysis as images to be compared are closer together and it is useful for presentation as it saves space. This type of visualization was previously performed manually by domain experts.

4.2. The reflection (mirroring) feature

A sedimenting ellipse can rotate clockwise or counterclockwise depending on the initial arrangement of the surrounding bubbles. Similarly, for the interacting discs, the left disc can move around the right disc or vice-versa. Domain experts would like to better compare datasets that have mirrored features such as a sedimenting ellipse or sedimenting discs that rotate in different directions. To address this requirement, we provide a user option that reflects a view about a vertical (or horizontal) axis that passes through the middle of simulation bounding box.

4.3. Linked Time with Event Synchronization

In a simulation that involves objects interacting with foam, the object's movement in the simulation is controlled by an *effective time scale*, which specifies how much an object is moved (in the direction of the resultant force) at each time step. This parameter may be different for different simulations which means that objects with similar behavior may move at different speeds. Even for simulations with the same effective time scale, we want a similar event in both simulations to happen at the same time so that behavior up to that event can be compared and analyzed together. Examples include comparing two constriction simulations with different flow rates or comparing the sedimenting discs with the sedimenting ellipse simulations. When comparing the sedimenting discs with the sedimenting ellipse simulations, the ellipse

and the discs start in similar configurations. The main axis of the ellipse and the line connecting the center of the two discs are horizontal. We want the ellipse and the discs to reach intermediate configurations and the stable configuration at the same time. These configurations are defined in terms of the angle that major axis of the ellipse and the line connecting the centers of the two discs make with a horizontal line. For instance, the intermediate configurations could be defined as angles: $0°$, $30°$, $60°$, and $90°$ which means that we want both the ellipse and the sedimenting discs reach these orientations at the same time.

The *linked time with event synchronization* addresses these requirements. This technique allows the user to specify time steps in each simulation when significant events happen. The following requirements hold: (i) all simulations have the same set of events; (ii) events are ordered per simulation based on time of occurrence; (iii) corresponding events in different simulations have the same event index. This technique ensures that corresponding events in different simulations are shown at the same time. For each time interval v_{ij} before an event i, one simulation will run at its normal speed (the simulation with the maximum time interval before event i denoted v_{iL}), all other simulations will be "slowed down" (v_{ij} simulation steps will be displayed in v_{iL} time steps). This results in event i being shown simultaneously in all simulations. If we were to "speed up" rather than "slow down" simulations this would result in skipped time steps which in turn results in lost precision. Simulations run at normal speed for the interval after the last event. We formalize our technique next.

Multiple-linked views are used to show a different simulation in each view. Let us assume that the first time step is 0 and let t_j be a time step in simulation j where $0 \le j < s$, and s is the number of simulations. The time for all linked views is specified using a common *linked time t_L*. The linked time is converted to simulation time t_j which is used to load the specified simulation time step. FoamVis uses the following default setup for linked time t_L: one time step in the first simulation corresponds to one time step in every other simulation. That means that, by default, all simulations run at their default speed. This default setup is modified if the user desires to examine the context of related events in different simulations.

To specify events of interest the user unlinks the time parameter for the multiple views. After this operation, time can be changed independently for each view. The user specifies times t_{ij} at which event i occurs in simulation j ($0 \le i < n$, n is the number of events and $0 \le j < s$, s is the number of simulations), then the user links the time in the s views. Let t_L be the linked time. We analyze how the linked time t_L is converted to simulation time t_j for simulation j.

Let v_{ij} be the time interval between events $i-1$ and i for simulation j, if $i > 0$; or the time interval before event i if

$i = 0$. We have that

$$v_{ij} = \begin{cases} t_{ij} & \text{if } i = 0 \\ t_{ij} - t_{i-1,j} & \text{if } i > 0 \end{cases}$$

Let $v_{iL} = \max_{0 \le j < s} v_{ij}$, the maximum interval v_{ij} for event i and all simulations j. We denote by r_{ij} the ratio by which we "slow down" each simulation j for time interval before event i. We have that $r_{ij} = v_{iL}/v_{ij}$. In linked time, event i happens at time $t_{iL} = \sum_{k=0}^{i} v_{kL}$.

A simulation time t_j (for simulation j) can be deduced from the linked time t_L:

$$t_j = \begin{cases} \lfloor t_L/r_{0j} \rfloor & \text{if } 0 \le t_L < t_{0L} \\ t_{k-1,j} + \lfloor (t_L - t_{k-1,L})/r_{kj} \rfloor & \text{if } t_{k-1,L} \le t_L < t_{kL}, \\ & \quad 0 < k < n-1 \\ t_{n-1,j} + (t_L - t_{n-1,L}) & \text{if } t_{n-1,L} \le t_L \end{cases}$$

Using this approach, related events occur at the same common *linked time* in all s simulations, facilitating the comparison of their temporal context.

The average computation engine computes an average of simulations attributes over a time window behind the current time step. If linked time with event synchronization is used, the time window t_{WL} behind the current time step t_L is specified using the common *linked time*. Earlier we described how to compute the simulation time t_j from the linked time t_L. Similarly, the time window specified that uses the simulation time t_{Wj} (for simulation j, $0 \le j < s$, s is the total number of simulations) is derived from the time window that uses the linked time t_{WL}. Let us assume that the current time is between events $i-1$ and i, that is $t_{i-1,L} \le t_L < t_{jL}$. Let us also assume that the beginning of the time window falls between events $k-1$ and k, that is $t_{k-1,L} \le t_L - t_{WL} + 1 < t_{kL}$. We have that the time window t_{Wj} for simulation j can be computed from the common time window t_{WL} using the following equation:

$$t_{Wj} = \lfloor (t_{kL} - (t_L - t_{WL} + 1))/r_{kj} \rfloor + \sum_{l=k}^{i-1} v_{lj} + \lfloor (t_L - t_{i-1,L})/r_{ij} \rfloor$$

where v_{ij} is the time interval before event i in simulation j and r_{ij} is the ratio by which we slow down simulation j for the interval between events $i-1$ and i.

4.4. Force Difference and Torque Visualizations

The forces and the torque acting on objects are computed by the simulation code and stored in the simulation data. For the sedimenting discs simulation, the interplay of the network and pressure forces rotate one disc around the other. We provide a user option that displays the difference between the forces acting on the leading disc and forces acting on the trailing disc. This difference allows us to better analyze the causes of the rotation as there is a direct correspondence between the forces displayed on the screen and the movement of the disc (Fig. 8b right).

The torque $\vec{\tau}$ rotating an object around its center is displayed as a force $\vec{F}$ acting off-center on the object $\vec{\tau} = \vec{r} \times \vec{F}$, where $\vec{r}$ is the displacement vector from the center of the object to the point at which the force is applied. The distance $|\vec{r}|$ is a user-defined parameter, FoamVis calculates the appropriate value of $\vec{F}$ to keep the torque at its given value (Fig. 8 left).

5. Visual Analysis

We start with an overview of the processing and visualization solutions provided. We process bubble edges that lie on the zero level set of a function such that we accurately represent foam channels and objects interacting with foam. Previously, we represented this kind of edges as line segments [LLCD11], now they can have an arbitrary shape as described by the function in the simulation file. This eliminates aliasing problems (such as for bubbles at the corners of the constriction simulation, Fig. 4 and 5 in Lipsa et al. [LLCD11]) and enables analysis of new datasets (such as the sedimenting ellipse simulation) because we can accurately represent objects boundaries. We compute a deformation tensor which encodes both the value and direction of deformation. Both measures are important for validating simulations against experiments. We provide visualizations for tensor and vector data. We provide time-averaged computation of simulation attributes to smooth out the high fluctuations in attribute values caused by topological changes and provide a high level view of the foam dynamics. We provide visualizations of objects interacting with foam. Foam attributes around a dynamic object determine the forces acting on that object and ultimately the behavior of the object interacting with foam. To illustrate the distribution of plasticity in foam, we compute a kernel density estimate (KDE) for the locations of topological changes. With this visualization we address over-plotting issues present if we just render the location of each topological change.

Note that we use consistent color maps throughout this work: diverging color maps blue-red for deformation, blue-tan for pressure, purple-orange for velocity and a sequential color-map white-blue for the kernel density estimate.

5.1. Deformation Tensor Computation and Visualization using Ellipses

While visual inspection of individual bubbles provides information about foam deformation, this information is not quantified, and, more importantly, cannot be averaged to obtain the general foam behavior. To address these issues, we compute the bubble deformation measure as defined by Graner et al. [GDRM08]. Let i and j be two neighboring bubbles (which share an edge), let C_i and C_j be their centers and assume that the vector $\overrightarrow{C_iC_j}$ has components (x,y). We

define a tensor $\mathbf{T_{ij}}$ as the direct product of $\overrightarrow{C_iC_j}$ with $\overrightarrow{C_iC_j}$.

$$\mathbf{T_{ij}} = \overrightarrow{C_iC_j} \otimes \overrightarrow{C_iC_j} = \begin{pmatrix} x^2 & xy \\ xy & y^2 \end{pmatrix}$$

The deformation tensor $\mathbf{T_i}$ for bubble i is defined as $\mathbf{T_i} = \sum_{j=1}^{n} \mathbf{T_{ij}}/n$ where n is the number of neighbors of bubble i. This tensor is positive definite symmetric (each element of the average is positive definite symmetric) so it has positive eigenvalues. The deformation tensor is represented by an ellipse [GDRM08] that has each axis' length and direction given by the tensor's corresponding eigenvalue and eigenvector. This representation shows both deformation value (ellipse eccentricity) and direction (the orientation of the ellipse) and can be averaged over an area and over time. We use these properties to show large scale (general) deformation behavior in foam obtained by time-averaging bubble-scale behavior.

In 2D, the standard measure [LLCD11] is computed by $P/\sqrt{A}$ where P is the bubble's instantaneous perimeter and A is its area. We add a new scalar measure of deformation given by the ellipse anisotropy [GDRM08]: $1 - s_2/s_1$ where s_1 and s_2 are the (positive) eigenvalues of the deformation tensor with $s_1 > s_2$. This scalar improves on the standard deformation measure which depends on the number of sides of a bubble.

5.2. Time-Average Computation and Visualization

Bubble-scale simulations are used to model foam properties and study their influence on macroscopic behavior of foam. However, this fine level of detail, the fact that bubbles are discrete, and the large fluctuations in bubble attribute values generated by topological changes can make understanding of general trends in foam behavior very difficult. A good way to smooth out these variations is to calculate the average of attribute values over time. This results in fewer changes between time steps as well as smooth changes between neighboring areas of the foam. Both these effects facilitates the observation of general trends in data.

FoamVis [LLCD11] includes a time-average computation engine for scalar simulation attributes. We extend the average computation engine in three ways. First we integrate the linked time with event synchronization with the time-average techniques. Second we support other types of simulation attributes such as vectors and tensors and, third we allow each time step to have a variable number of sub-steps which is required for computing topological changes KDE (Section 5.4).

We use the time-average computation engine to compute an average over a time window of a tensor field such as the bubble deformation (Section 5.1) or of a vector field such as the bubble velocity, defined as the motion of the center of mass. We average tensors by averaging over time each array used to store a tensor at a given position. We average vectors
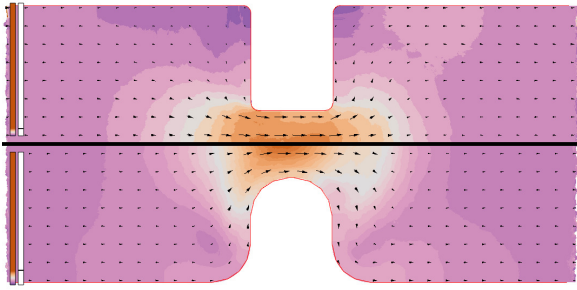
Figure 4: We show the square (top) and rounded (bottom) constriction simulations. Velocity is shown with glyphs, velocity magnitude is color-mapped and it is mapped to the size of the glyph. An average over the entire duration of the simulations is displayed. Rounding the corners of the constriction results in the disappearance of the areas of stagnated bubbles visible in the top corners of the square-constriction as dark purple regions. Note that the color bar shows mostly the color associated with high values (orange) because of clamping.

by averaging over time each vector component for the vector at a given position. We visualize the tensor field using glyphs and the vector field using glyphs and streamlines.

A visualization for the field produced by the average computation is done by dividing the field into a Cartesian grid. The center of each square tile is sampled and the attribute value for that texel is displayed. The position and resolution of the grid are user adjustable parameters, which is useful for sampling the field at different positions. Other sampling strategies for the tile are possible, for instance taking an average of all texels in the square.

The tensor is visualized using an ellipse (Fig. 2) that has each axis length and direction given by the deformation tensor's eigenvalue and eigenvector. The vector is visualized using an arrow with length proportional to the vector magnitude (Fig. 4), with an arrow with fixed length or with streamlines (Fig. 7).

Velocity vectors have a wide range of values because the velocity of bubbles involved in topological changes can be much larger than the average velocity of the flow. To address this issue, the arrow length is clamped to a maximum value with clamping shown in a *length bar*. The height of the length bar encodes the maximum vector magnitude while the horizontal line inside the bar shows the clamping value (Fig. 4).

5.3. Temporal-Averaging of Bubble Attributes around Moving Objects

For foam simulations that include moving objects, we are interested in the forces that determine objects' behavior. These
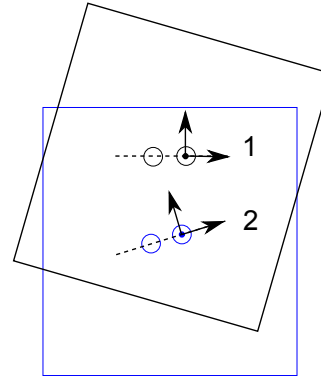
(a)
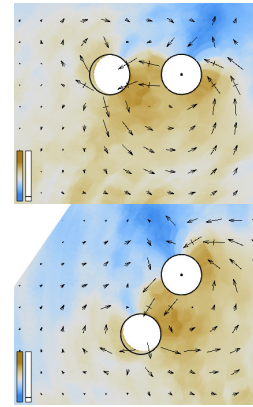
(b)

Figure 5: Average around dynamic objects interacting with foam. (a) The two discs start in position 1, and reach position 2 at $t = 50$. To compute the average around the two discs, the texture for the current time step D_t is transformed before it is added to the sum S such that the coordinate system at position 2 overlaps the coordinate system at position 1. (b) Average around two discs for $t = 99$ and a time window of 19. We show the two objects without (top) and with (bottom) the *show rotation* feature.

forces are determined by properties of the bubbles adjacent to the objects. However, examining bubble attributes around objects for every time step is not always the best option. There is too much detail and bubble attribute values have large fluctuations caused by topological changes. To address this issue, we compute a temporal average of attribute values *around* the dynamic objects using the approach of Lipşa et al. [LLCD11]. We extend that work by supporting simulations with objects that undergo general transformations, computing average around two objects and providing the *show rotation* feature that provides the context for dynamic objects.

We keep fixed the coordinate system attached to the ob-

ject. We render the simulation data for a time step in a floating point texture D_t such that each texel covered by a bubble stores the bubble's attribute value. We compute a texture S as the sum of textures D_t for a time window behind the current time-step. Before the texture for the current time step D_t is added to the current sum of textures S, we transform it (translate and/or rotate) so that the object coordinate system stays fixed. As an example, Fig. 5a shows the *sedimenting-discs* simulation with the two discs starting side-by-side in position 1. The user chooses to show an average around both discs, expecting that the two discs move as a system. The right disc is fixed for the average, and the left disc specifies the rotation of the two discs. At $t = 50$, the discs reach position 2, where both discs descend and the disc on the left starts the rotation around the disc on the right. Before the texture for the current time step D_t is added to the current sum of textures S, it is transformed so that the coordinate systems in positions 1 and 2 overlap. Note that when averaging tensor and vector attributes, those have to be rotated with the same rotation angle before they are stored in the texture D_t.

Fig. 5b top shows the average around the two discs for time steps 80 to 99. While this image has the correct foam properties around the two objects, it does not contain information about the position of the two objects in space. To address this we offer the *show rotation* option which rotates the computed average so that it matches the actual position of the two objects in space (Fig. 5b bottom). Contrast Fig. 5b bottom with Fig. 13-middle in Lipsa et al. [LLCD11], where the scalar average is not correct for the rotating disc because scalars are averaged only around the top disc.

5.4. Topological Changes Kernel Density Estimate (KDE)

Topological changes, in which bubbles change neighbors, show plasticity in foam. Domain experts expect that their distribution will be an important tool for distinguishing and validating simulations. Simply rendering the position of each topological change suffers from over-plotting, so it may paint a misleading picture of the real distribution (see Fig. 7-bottom in Lipsa et al. [LLCD11]). We adopt the method of Daae Lampe and Hauser [DLH11] to compute a KDE for topological changes (Fig. 6 and Fig. 3 (b)). While traditional histograms show similar information and are straightforward to implement they have drawbacks which may prove important depending on the context, including the discretization of data into bins (which may introduce aliasing effects) and the fact that the appearance of the histogram may depend on the choice of origin for the histogram bins [DLH11]. Kernel-based methods for computing the probability density estimate eliminate these drawbacks.

In foam simulation data, each topological change has two properties specifying when and where the topological change occurred. For each topological change, we place a
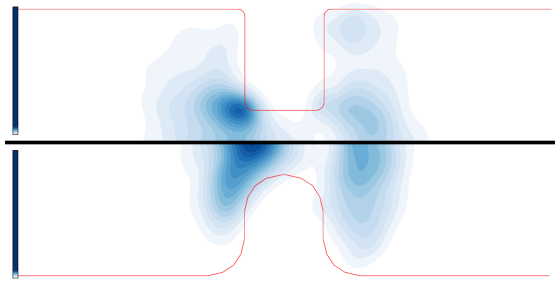

Figure 6: Comparison of topological changes KDE. We show the square (top) and rounded (bottom) constriction simulations using the *two halves view*, foam flows from left to right. Rounding the corners of the constriction results in the upstream region of concentrated topological changes moving towards the center of the constriction and downstream. Note as well a region of topological changes in the downstream corners of the square-constriction.

2D Gaussian at the T1's position and add it to the sum of textures S. The KDE is computed by dividing by the number of time steps. The standard deviation for the Gaussian is a user defined parameter which determines the amount of detail that is visible in the final visualization.

6. Results

Our tool is developed in close collaboration with the foam scientists who design and run these simulations. We present case studies describing the way in which they use FoamVis, and the insights that they gain.

6.1. What is the effect of varying the shape of the constricted channel on the elastic and plastic deformation in a flowing foam?

Fig. 2 shows the deformation, averaged over the entire duration of the simulations, using the *two halves* view. Here, we visualize the elastic response of the foam and how it is affected by the roundness of the corners of the constriction. Rounding the corners results in reduced elastic deformation of the foam. In the square-constriction, foam is highly compressed both upstream, as bubbles are pushed against the wall, as well as downstream, as bubbles detach from the wall. This does not occur to the same extent in the rounded-constriction (independent of the length of the constricted region). An area where bubbles are not deformed can be observed just downstream from the constriction in both simulations. Here bubbles move from an area where they are deformed flow-wise (inside the constriction) to an area where they are deformed span-wise (downstream from the constriction).

Comparing Fig. 2 and 6 shows that only in the square constriction are the bubbles attached to the wall downstream of

the constriction significantly stretched, which gives rise to a higher density of topological changes as they occasionally detach. In the rounded constriction, the bubbles slide around the wall (Fig. 4), do not get stretched, and do not trigger topological changes.

As the original FoamVis provided only a visualization for the deformation scalar and locations of topological changes, this analysis would have been difficult. The deformation scalar does not indicate the direction in which bubbles are deformed and the direct visualization of topological changes suffers from over-plotting.

6.2. Do we have circulation and regions of stagnated flow in a constriction?

There have been a number of studies of foam flow through a constriction (see the review of Jones et al. [JDS*11]), but none have ever found recirculation. Most recently, Jones and Cox [JC12] examined both long-time averages and instantaneous vector plots of the velocity and concluded that vortices were not present in any of the different constriction geometries that they examined.

A subset of this data was re-examined using FoamVis, which offers the possibility to easily change the time-window over which the velocity field is averaged and can show streamlines to facilitate observation of recirculatory behavior for one time step. As Fig. 7(a) shows, over intermediate time-scales (here 50 time-steps) recirculation appears to occur. However, only a few individual time steps show recirculation, and here it is caused by topological changes (Fig. 7(b)). So the effect of the time average is to dilute this circulatory motion, but clearly it does not completely do so. Further, Fig. 7(c) shows that an individual step can show recirculation in the absence of topological changes, a surprising and potentially significant finding, although the bubble velocities are very small. Because simulations are quasi-static, i.e. foam is at equilibrium in each time step, a topological change in previous time steps cannot determine circulatory motion in the current time step. Because the circulation motion does not persist for many time steps bubble paths or pathlines/streaklines do not show it.

In the rounded constriction, there is much less recirculation, which is presumably related to the decrease in the density of topological changes.

This new finding stimulates further questions. With access to more data, we hope to be able to answer questions about circulations' persistence when parameters such as bubble size and polydispersity and constriction shape are varied.

The velocity field visualization (Fig. 4) shows clear differences between the flow in both geometries. The "dead zones" from the foam are only visible in the top corners of the square-constriction as dark purple regions. Rounding the corners results in the disappearance of these stagnated bubbles.
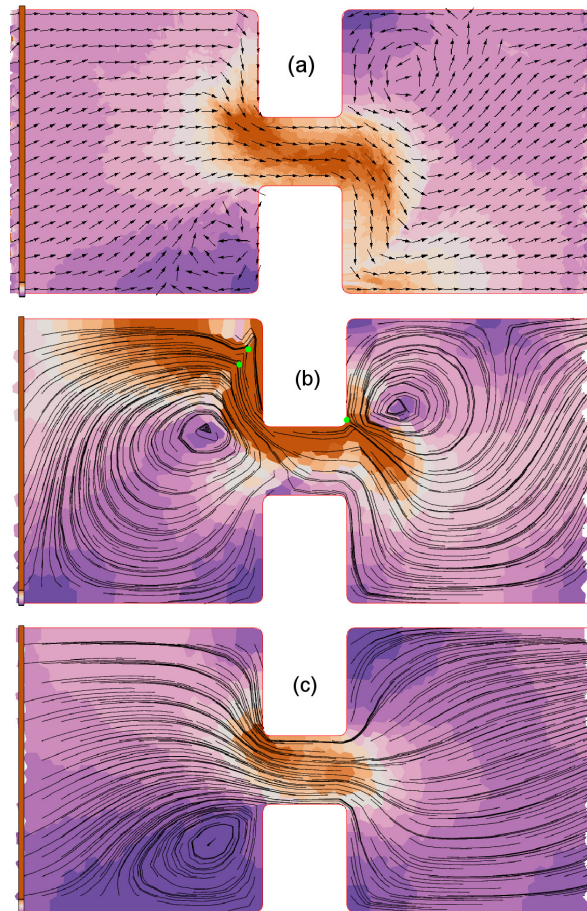

Figure 7: (a) Velocity is shown with glyphs of the same size. An average over 50 time steps is computed, for both velocity vectors and velocity magnitude, $t = 441$. The visualization shows apparent circulation of bubbles within the square-constriction flow (bottom-left and top-right). (b) Topological changes are shown with green dots, velocity field is shown with streamlines, $t = 412$. Topological changes cause strong circulation movement. (c) Velocity is shown with streamlines, $t = 417$. We show circulation of bubbles not caused by topological changes, a result never presented before. For all figures velocity magnitude is color-mapped (orange is for high and purple is for low velocity magnitude).

6.3. Can we approximate the sedimenting-discs behavior with the sedimenting ellipse behavior?

We probe a foam's response to the sedimentation of solid objects with the aim of being able to predict the path and residence time of an object in a foam. This has application in industrial processes such as froth flotation for ore separation. We consider the sedimentation of two interacting circular discs and an ellipse in a dry monodisperse foam.

The interaction between two circular discs sedimenting in a dry foam is such that they reach a stable configuration in which they are directly above one another and separated by (roughly) two bubbles. Thus when discs are initially side-by-side in the foam, they rotate about one another into this stable configuration. They interact in this way as long as they are within a critical separation of each other. The critical separation is dependent on whether the region where topological changes are concentrated around each disc are merged [DC09]. We wish to understand the extent to which this result can be related to the similar but simpler result; that of a sedimenting ellipse in a foam. An ellipse that is initially horizontal in the foam rotates so that it becomes vertical during sedimentation. The main driving force behind this process is the torque exerted on the ellipse by the films as they bunch up at an off-center position on the ellipse's boundary [DC10].

Fig. 3 (a) shows how the flow of foam is similar when the orientations of the objects match each other. We note that bubbles in-between the two discs are moving at a high velocity, with the discs. We previously noted that this is a region in the foam where bubble deformation is lower than expected [LLCD11]. We also note that compared to regions such as the wake of the trailing disc and in front of the leading disc, fewer topological changes occur between the discs (Fig. 3 (b)). As a result, the foam behaves (mainly) as an elastic solid in between the two discs. This results in the two discs behaving as a single object in the foam. In this case, one would expect the two discs to behave similar to a longer object such as an ellipse.

The elastic deformation (Fig. 8) caused to the foam by both types of objects has some similarities: Regions of high deformation appear in the wake (where bubbles are stretched vertically) and in front of the objects (where they are squeezed horizontally). The pressure field is also very similar in both cases (Fig. 8). For example, Figure 8a left shows a region of high pressure mainly on the right side underneath the ellipse which contributes to the drift of the ellipse toward the left wall. Similarly, for the two discs (Fig. 8a right), the pressure is higher underneath the right hand disc resulting in a greater pressure drag being exerted on it, which contributes to the initial faster descent of the disc on the left.

However, there are also clear differences: For the ellipse, the region of high deformation in the wake is always positioned at the highest point of its boundary. Once it is tilted slightly from its initial orientation (due to the disorder of the foam) this region moves to an off-center position. Films become bunched up together here and contribute to a large network force that drives the rotation (Fig. 8b left). Note here that a smaller pressure force opposes the rotation of the ellipse. This is a different mechanism to what is driving the rotation of one disc around the other. The force difference tool (see Fig. 8b right) shows that both the network and the
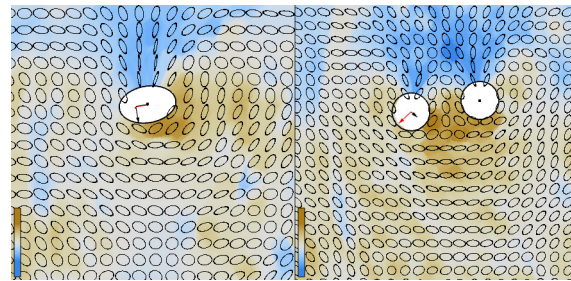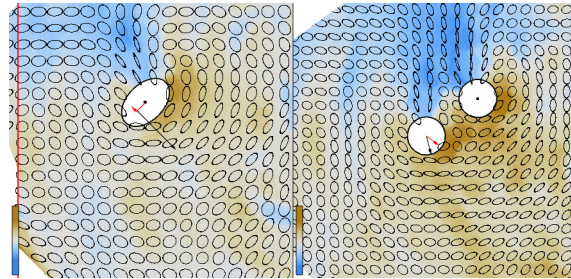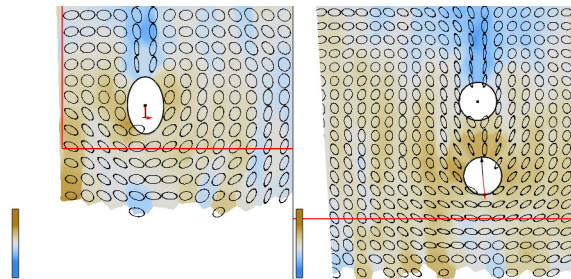

(a) Beginning of the simulation, $t = 133$.

(b) Rotation phase, $t = 283$

(c) Stable orientation, $t = 1169$

Figure 8: Sedimenting-ellipse versus sedimenting-discs. The *linked time with event synchronization* feature is used to synchronize the rotation of the ellipse and the two discs such that they reach an orientation of $45°$ at the same time. Attributes (pressure, deformation and forces) are averaged over 52 time steps for the ellipse simulation (resulting in an average over 15 time steps for the two disc simulation). Pressure is color-mapped (tan for high and blue for low pressure), deformation is shown using ellipses. The force *difference* between the leading disc and the trailing disc and the torque on the ellipse is indicated. The network force and torque are indicated with a black arrow and the pressure force and torque are indicated with a red arrow. The channel wall can be seen in Fig. (b) left and Fig. (c) left; Fig. (c) bottom shows the lower, periodic boundary of the foam.

pressure forces contribute to the rotation of one disc around the other.

The objects continue to rotate into their stable configura-

tion and once they become oriented so that they are vertically aligned, both the pressure and deformation fields become symmetric (see Fig. 8c). The stability of these orientations is confirmed by the force visualizations: the resultant torque on the ellipse and force difference on the discs are each close to zero. The combined visualizations shown in Fig. 8 allow us to probe the different contributions of network and pressure forces on these two similar results.

To fully understand the *sedimenting-discs* simulation, we must collate more simulations in which the initial separation between the two discs and the disc size as well as the ellipse eccentricity and size are varied. We know [DC10] that changing the ellipse's eccentricity and size changes its rate of rotation and that changing the disc separation and size affects the rate at which they rotate around each other [DC09]. We want to know which combination of parameters results in the most similar behavior for both types of simulation, which would allow us to further compare and contrast the two simulations.

6.4. New simulation parameters chosen using FoamVis.

Noting the similarities between the sedimenting discs and the sedimenting ellipse simulations, we use FoamVis to decide on new simulation parameters. Here we aim to predict the size and shape of the ellipse required to obtain a similar rate of rotation to the two discs in the foam. The similarities in the flow field for both simulations shown in Fig. 3 (a) suggest that by choosing a larger and more eccentric ellipse, we should obtain better matching simulations. We propose that an ellipse with an area of at least ten times the bubble area and an eccentricity of 0.7 will be adequate. These parameters are chosen so that the shape of the ellipse can be fitted to cover the two discs and the elastic region of foam in-between. (In Fig. 3 (a), the ellipse has an area of four times the bubble area and an eccentricity of 0.8.) The larger, more eccentric ellipse experiences a greater torque [DC10] in the foam and therefore rotates at a greater rate during sedimentation.

7. Conclusions and Future Work

We describe solutions designed to facilitate comparison of related foam simulations and enhance foam scientists' analysis capabilities. The effectiveness of our visualization solutions is demonstrated through new findings and a new approach to analyze the sedimenting discs simulation. Both these results generate new hypotheses for domain experts. We propose a new interaction technique that enables the comparison of related events in different simulations and facilitates the examination of their temporal context.

For future work, we want to compare simulations with experiments and provide visualizations for 3D foam simulations and experiments.

References

[AHP*10] AHRENS J., HEITMANN K., PETERSEN M., WOODRING J., WILLIAMS S., FASEL P., AHRENS C., HSU C.-H., GEVECI B.: Verifying scientific simulations via comparative and quantitative visualization. *IEEE Computer Graphics and Applications 30*, 6 (nov.-dec. 2010), 16 –28. 2

[DC09] DAVIES I., COX S.: Sedimenting discs in a two-dimensional foam. *Colloids and Surfaces A: Physicochemical and Engineering Aspects 344*, 1-3 (2009), 8–14. 10, 11

[DC10] DAVIES I., COX S.: Sedimentation of an Elliptical Object in a Two-Dimensional Foam. *Journal of Non-Newtonian Fluid Mechanics 165*, 13 (2010), 793–799. 10, 11

[DLH11] DAAE LAMPE O., HAUSER H.: Interactive Visualization of Streaming Data with Kernel Density Estimation. In *Pacific Visualization Symposium (PacificVis)* (2011), IEEE, pp. 171–178. 8

[GDRM08] GRANER F., DOLLET B., RAUFASTE C., MARMOTTANT P.: Discrete Rearranging Disordered Patterns, Part I: Robust Statistical Tools in Two or Three Dimensions. *The European Physical Journal E: Soft Matter and Biological Physics 25*, 4 (2008), 349–369. 6

[JC12] JONES S., COX S.: On the Effectiveness of a Quasi-Static Bubble-Scale Simulation in Predicting the Constriction Flow of a Two-Dimensional Foam. *J. Rheol. 56* (2012), 457–471. 9

[JDS*11] JONES S., DOLLET B., SLOSSE N., JIANG Y., COX S., GRANER F.: Two-dimensional constriction flows of foams. *Colloids and Surfaces A: Physicochemical and Engineering Aspects 382*, 1-3 (2011), 18 – 23. 9

[LLC*12] LIPŞA D. R., LARAMEE R. S., COX S. J., ROBERTS J. C., WALKER R., BORKIN M. A., PFISTER H.: Visualization for the Physical Sciences. *EG Computer Graphics Forum 31*, 8 (Dec. 2012), 2317–2347. 2

[LLCD11] LIPŞA D. R., LARAMEE R. S., COX S. J., DAVIES I. T.: FoamVis: Visualization of 2D Foam Simulation Data. *Visualization and Computer Graphics, IEEE Transactions on 17*, 12 (Oct. 2011), 2096–2105. 2, 6, 7, 8, 10

[MHG10] MALIK M., HEINZL C., GROELLER M.: Comparative visualization for parameter studies of dataset series. *Visualization and Computer Graphics, IEEE Transactions on 16*, 5 (sept.-oct. 2010), 829 –840. 2

[PP95] PAGENDARM H., POST F.: Comparative Visualization - Approaches and Examples. In *Visualization in Scientific Computing*, Göbel M., Müller H., Urban B., (Eds.). Springer, Wien, 1995, ch. 2. 2

[PW95] PAGENDARM H.-G., WALTER B.: Competent, compact, comparative visualization of a vortical flow field. *Visualization and Computer Graphics, IEEE Transactions on 1*, 2 (jun 1995), 142 –150. 2